JOURNAL OF MATERIALS SCIENCE 7 (1972) 531–542

Dislocation Generation at Surfaces of Tin Single Crystals

R. FIEDLER*
Institute of Metallurgy, Czechoslovak Academy of Sciences, Žižkova 22, Brno, Czechoslovakia

A. R. LANG
H. H. Wills Physics Laboratory, The University, Bristol, UK

Single crystals of 99.999% purity β-tin grown from the melt were shown by X-ray topography to contain dislocations with Burgers vectors of [001] type and of $\frac{1}{2}\langle 111\rangle$ type. Specimen plates cut roughly parallel to (311) were chemically thinned from 1.25 mm to 100 μm thickness and in two cases characteristic dislocation structures were generated at their surfaces. A specimen thinned in concentrated HCl possessed stress-producing centres distributed on its surfaces with a density of about 75 mm^{-2} from which regular helices and coaxial prismatic loops with [001] Burgers vector were generated together with irregular loops of $\frac{1}{2}\langle 111\rangle$ Burgers vector dislocations. In one specimen thinned in a H_3PO_4, CH_3COOH, HF and HNO_3 mixture large arrays of pure edge dislocations grew parallel to the surface at a depth of 2 to 4 μm below it, the individual dislocations extending at about 1 $\mu m\ h^{-1}$ during several weeks. These edge arrays all had that one of the four $\frac{1}{2}\langle 111\rangle$-type Burgers vectors which made the smallest angle (5°) with the surface. The Burgers vector sense, determined by X-ray diffraction contrast, corresponded to a sheet of vacancies lying between the dislocation line and the surface.

1. Introduction

As part of an investigation into the dislocation structure within large, undeformed single crystals of tin, a variety of crystal-growing techniques based either on the strain-anneal method or on growth from the melt was explored. The method employed to map dislocations and to determine their Burgers vectors was X-ray topography. For the X-ray experiments it was necessary to reduce selected regions of specimens to thicknesses of about 100 μm, and it was desirable that an area of at least a few millimetres in diameter should be fairly uniformly of such thickness. A technique was devised for producing single crystals by the strain-anneal method with a thickness of 100 μm or less, these being located in circular "wells" of diameter 5 mm stamped or machined in a 0.5 mm thick strip about 5 cm long and 1 to 1.5 cm in width. The control of grain size achieved in these thin regions was not good and their rate of loss through accidental plastic deformation was high. The direct production of regions of the required thinness by a melt-growth technique which involved sucking the melt into a carbon-coated glass mould, in a modification of the technique previously applied to tin by Takaki *et al* [1], also resulted in an intolerable failure rate due to plastic deformation. Production of single crystals which would require no appreciable thinning before X-ray examination was therefore abandoned. As a consequence, the investigation became heavily dependent upon the successful operation of chemical and/or electrolytic thinning techniques for the preparation of specimens which would fairly represent the bulk material.

Following relaxation of the limit of 100 μm on the initial thickness, so that growth of crystals 0.5 mm thick or greater was permitted, it was found that crystals with a satisfactory freedom from low-angle boundaries and with a low overall dislocation density could be grown more easily from the melt than by the strain-anneal method, even though for the melt-growth experiments a

*Visitor to H. H. Wills Physics Laboratory under Royal Society–ČSSR Cultural Agreement.

simple, rigid graphite boat of the traditional Chalmers design [2] was used rather than a soft mould [3] from which fewer deforming stresses on the crystal would be expected. The superiority of the melt-grown crystals was unexpected in view of the report by Jaffrey and Chadwick [4] that sub-grains of diameter about 1 mm with small relative misorientations (less than 30″ of arc) were present throughout tin crystals prepared by a similar melt-growth procedure, their conclusion being based upon photographs taken with the Schulz X-ray reflection technique [5]. On the other hand Brümmer and Alex [6] had successfully prepared by the strain-anneal method large grains, some tens of mm² in area, substantially free from low-angle boundaries, and with a very low dislocation density as directly determined by the method of transmission X-ray topography [7].

In the tin single-crystal specimens described below a fair proportion of the dislocations observed was believed to have been introduced during the specimen thinning and mounting procedures. This origin was suggested by their configurations and, in some cases, by the nature of their movements from day to day. Those dislocations which arose simply from mechanical deformation were distributed fairly uniformly throughout the specimens except in regions where local deformation was obvious and the dislocation density consequently relatively high. There were also present in some specimens certain dislocation configurations attributable to sources at or near the specimen surfaces. These latter groups of dislocations were quite localised in occurrence. Among dislocations of this class two distinctive structures manifested themselves, occurring separately on different specimens. They were noteworthy as illustrations of two very different modes of dislocation line-length increase, both acting in response to forces generated by conditions at the specimen surface, and they were remarkable also for the scale on which they occurred. An analysis of the spatial arrangement of these dislocations, a time-lapse study of developing structures, and a determination of Burgers vectors of some of the dislocations involved constitute the topics of this paper.

2. Burgers Vector Identification

The Bravais lattice to which the β-tin structure belongs is body-centred tetragonal. Its parameters at 25°C are $a = 5.8315$Å, $c = 3.1814$Å, $c/a = 0.5456$, [8]. There are four atoms per unit cell, the atomic co-ordinates being (0, 0, 0), $(\frac{1}{2}, 0, \frac{1}{4})$ *et seq.* Indices of planes and directions will be referred to this body-centred tetragonal cell in the following discussion. The two shortest lattice translations are [001], and half the body diagonal, their respective magnitudes being $c = 3.18$Å and $\frac{1}{2}(2a^2 + c^2)^{\frac{1}{2}} = 4.42$Å. These, then, are likely Burgers vectors. The smallest, [001], is unique; of the next smallest there are four symmetrically equivalent of type $\frac{1}{2}\langle 111\rangle$. The energy of dislocation formation, but not necessarily the resistance to dislocation movement, would be smaller for the dislocations of lesser Burgers vector.

The X-ray topographs were taken under conditions of low absorption: in most regions studied the condition $\mu t \sim 1$ was satisfied (μ is the X-ray linear absorption coefficient, t is the crystal thickness). The radiation used was AgKα for which $\mu t = 1$ when $t = 86$ μm. Under these conditions the images of dislocations are weak or absent when $\mathbf{g} \cdot \mathbf{b} = 0$ ($\mathbf{g}$ is the reciprocal lattice vector of the Bragg reflection active). Dislocations with $\mathbf{g} \cdot \mathbf{b} = 1$ should be well visible and those with $\mathbf{g} \cdot \mathbf{b} = 2$ strongly visible.

The first concern of the X-ray topographic investigation was to assign dislocations to their respective Burgers vector type, i.e. [001] or $\frac{1}{2}\langle 111\rangle$. For this purpose the 200 and 020 reflections are important: in both of these reflections all dislocations having Burgers vectors with body-diagonal directions are visible, but for the c-axis Burgers vector $\mathbf{g} \cdot \mathbf{b} = 0$. Thus any additional lines appearing in reflections with the index l not equal to zero can be assigned to dislocations having a [001] Burgers vector. Such, and indeed all Burgers vector identifications, were always confirmed by examination of several topographs and by taking into account the character of the diffraction contrast produced by the dislocation, including in particular the width of the dislocation image. Reflections with indices $hh0$ are diagnostically most useful for establishing which of the four possible Burgers vectors of the set $\frac{1}{2}\langle 111\rangle$ a particular dislocation of this type possesses. In an earlier X-ray topographic study of dislocations in a body-centred cubic metal, Fe-3½% Si, in which specimen foils with surfaces parallel to (110) were examined, the $1\bar{1}0$ reflection could be recorded by symmetrical transmission, and four more reflections of the required type, 011, 101, $10\bar{1}$ and $01\bar{1}$, were equally accessible by asymmetrical transmission [9]. In tin the reflections with indices $hh0$ it would

be desirable to record are 220, $2\bar{2}0$, 101, 011, $\bar{1}01$ and $0\bar{1}1$ (or, of course, their inverses). The range of orientations of specimen surface with which it is likely to find more than half of these reflections easily accessible for transmission X-ray topographs is quite restricted. However, it is in principle sufficient to observe the relative visibility in only two of these six reflections in order to determine which of the four $\frac{1}{2}\langle 1\,1\,1\rangle$ type Burgers vectors is possessed by a given dislocation visible in 200 type reflections, provided the two reflecting planes used contain one body diagonal in common. Still, confirmatory evidence is desirable and this can always be obtained from some of the eight equivalent reflections of type $2h, h, h$ or from the four equivalent reflections of type $h, h, 2h$. All these dislocation visibility considerations bear upon the selection of useful orientations of specimen surface relative to the crystallographic axes; for the degree of accessibility of diagnostically valuable reflections determines the completeness with which the Burgers vectors of the dislocation population in a given specimen can be identified.

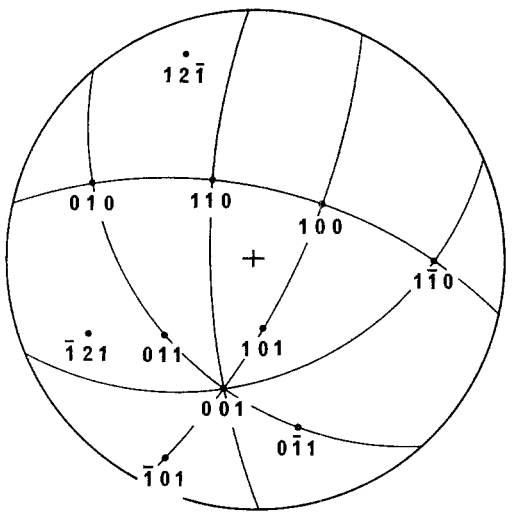

Figure 1 Stereographic projection on the plane of the specimens showing poles of useful Bragg-reflecting planes for Burgers vector identification.

Fig. 1 shows the orientation of the specimens used in the present work. Poles of planes important for Bragg reflections are indicated. Apart from the four planes (100), (110), (101) and (011) whose poles are nearest the centre of the projection, all the rest were usable for transmission X-ray topography; but not every specimen required examining in all these reflections. The five great circles in fig. 1 are the important crystallographic zones containing respectively the c-axis, and the cell base edges and cell base diagonals which are normal to the c-axis. The projection in fig. 2 shows, underlined, the *directions* of likely Burgers vectors. The great circles in this figure are the five "zones of invisibility" on which lie the poles of planes in whose Bragg reflections the condition $\mathbf{g} \cdot \mathbf{b} = 0$ obtains for one of the five Burgers-vector directions plotted. During the course of Burgers vector identification the projection in fig. 2 was found very helpful. The projections were constructed from the angle computations of Bradford and Vieth [10] and Woodyatt and Bradford [11].

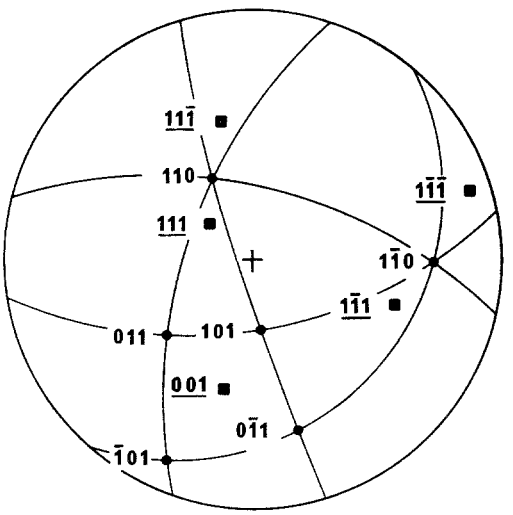

Figure 2 Stereographic projection on the plane of the specimens. Underlined are directions of likely Burgers vectors. The five great circles are the "zones of invisibility" containing planes for which $\mathbf{g} \cdot \mathbf{b} = 0$ for each of the five $\mathbf{b}$ vectors, respectively.

3. Specimen Preparation

The starting material was 99.999% grade polycrystalline tin ingot supplied by Metals Research Ltd. Prior to its use for growing single crystals this material was treated as follows. Lumps weighing a few hundred grams were melted under vacuum in a glass apparatus arranged so that the melt would pass through an orifice and oxide scum would be held back. The metal, thus filtered, then ran into clean glass tubes which were sealed under vacuum and not opened until

the crystal-growing boat was ready for charging.

The single crystals were grown at rates of about 0.5 mm per min under a temperature gradient of 5°C per cm. The rate of cooling down to room temperature averaged 1°C per min. A good vacuum was maintained during the whole process of heating, solidifying, and cooling to room temperature. The graphite boat was contained in a continuously pumped Pyrex glass vessel with a liquid nitrogen trap between it and the mercury diffusion pump. The slab-shaped crystals grown were 18 × 7 mm in cross-section over a length of 4 to 5 cm. Slices having the chosen orientation were cut from the slabs by an acid thread saw, a slice thickness not less than 1 to 1.25 mm being cut in order to avoid risk of plastic deformation during sawing. The required reduction of specimen thickness down to about 100 μm was generally performed more successfully by chemical thinning and polishing than by electrolytic polishing, as far as the avoidance of accidental plastic deformation was concerned. The specimens whose dislocation structures are described in sections 4 and 5 below were prepared from adjacent slices cut from the same crystal. They were both chemically thinned, but by different methods. One specimen, hereafter referred to as specimen A, was suspended in concentrated hydrochloric acid (specific gravity 1.18) for 95 h. This was not a satisfactory method of thinning, for it produced a large-scale roughness of the surface. The other specimen, B, was thinned for 6 h in a mixture of acids with volume ratios as follows: 60 parts orthophosphoric acid (sp. gr. 1.75), 25 parts glacial acetic acid, 10 parts hydrofluoric acid (approx. 40%), and 5 parts nitric acid (sp. gr. 1.42).

After thinning, specimens A and B were both chemically polished with the same acid mixture "L2" that Brümmer and Alex [6] used for polishing their tin crystals; but, after considerable experimentation, a polishing and rinsing procedure rather different from theirs was adopted. The L2 mixture differs from the thinning mixture used on B by omitting acetic acid and by combining the other three acids in the volume ratios: 57 parts H_3PO_4, 29 parts HF and 14 parts HNO_3. Its action is vigorous. The polishing procedure using L2 which was found to be most successful involved the following sequence of actions:

(1) Immerse specimen in L2 at 25°C until many bubbles form.

(2) Take specimen out of L2 and hold it in air until it becomes covered by a foam of bubbles. (If no foam forms, duration of immersion in L2 was inadequate.)

(3) Wash in de-ionised distilled water with slow agitation until a white precipitate forms on the specimen surface. It takes about 15 sec to do so.

(4) Rinse in fresh, concentrated H_3PO_4 until the precipitate starts to dissolve. This takes only about 2 sec: longer rinsing in H_3PO_4 causes surface roughening.

(5) Rinse in de-ionised distilled water for 2 sec.

(6) Rinse in N/50 $Ba(OH)_2$ for 2 sec.

(7) Make two rinses in de-ionised distilled water, each of 10 sec duration.

(8) Rinse in methanol for 10 sec.

(9) Dry in a non-oxidising atmosphere: a stream of 10% hydrogen, 90% nitrogen-gas mixture may be used for this purpose.

4. Dislocation Loops and Helices

The highly unsmooth surface produced on specimen A by the non-uniform thinning action of hydrochloric acid did not show any obvious crystallographic facetting. It did, however, exhibit irregular grooves and ridges, about 0.25 mm in length parallel to their long axes. Their general alignment on the surface lay in a direction perpendicular to [001], and there were some ridges which appeared to be bounded on one side by steep slopes in the vicinity of (001) orientation. The variations in specimen thickness produced a pronounced mottling of the background intensity on the X-ray topographs. This was due to the thickness-dependence of perfect-crystal integrated Bragg reflection intensity which occcurs in the transmitted-beam (i.e Laue) arrangement because of Pendellösung interference. Pendellösung fringes, which are the X-ray equivalent of the equal-thickness fringes familiar in transmission electron microscopy, function usefully as thickness contours. In crystals of relatively high electron density, such as metal crystals, the Pendellösung depth period (or the closely related quantity, the X-ray extinction distance) is of the order of 10 μm for the lowest-order reflections [9, 12]. The Pendellösung fringe order, counted from a hole or a tapered edge of the specimen (or at low-angle boundaries if such cross the region of interest [13]) can give a measure of local specimen thickness precise to 1 or 2 μm provided the specimen is free from inhomogeneous strain. Figs. 3a and b show a region of specimen A where the mean thickness was ~ 85 μm. Another region of A, shown in figs. 4a and b, was rather more non-

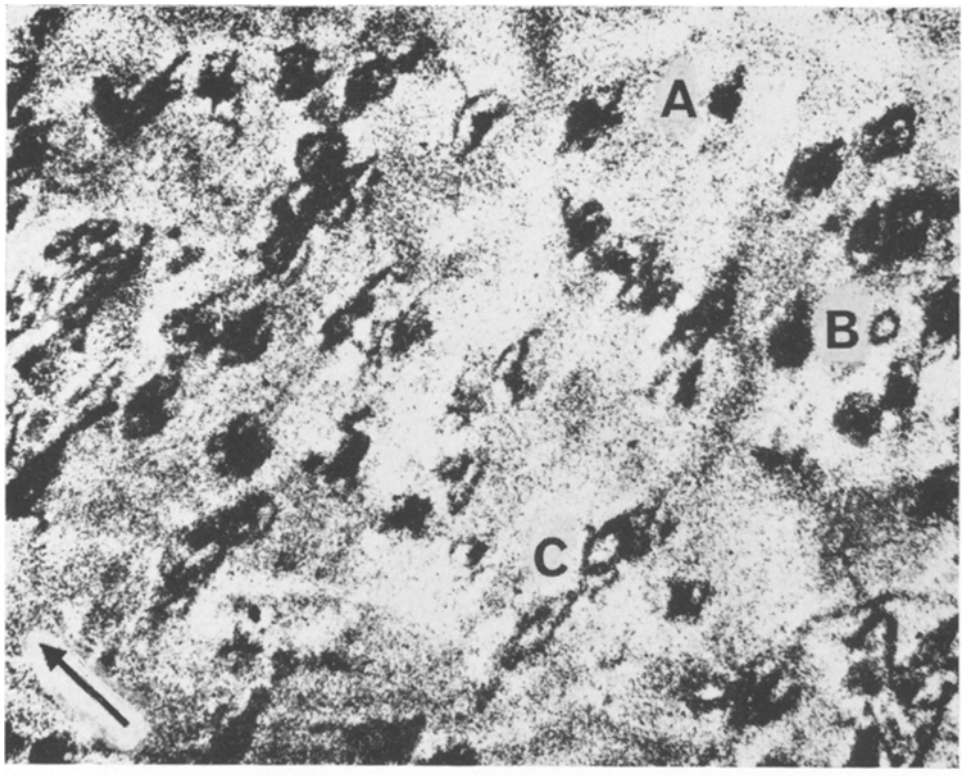

(a)

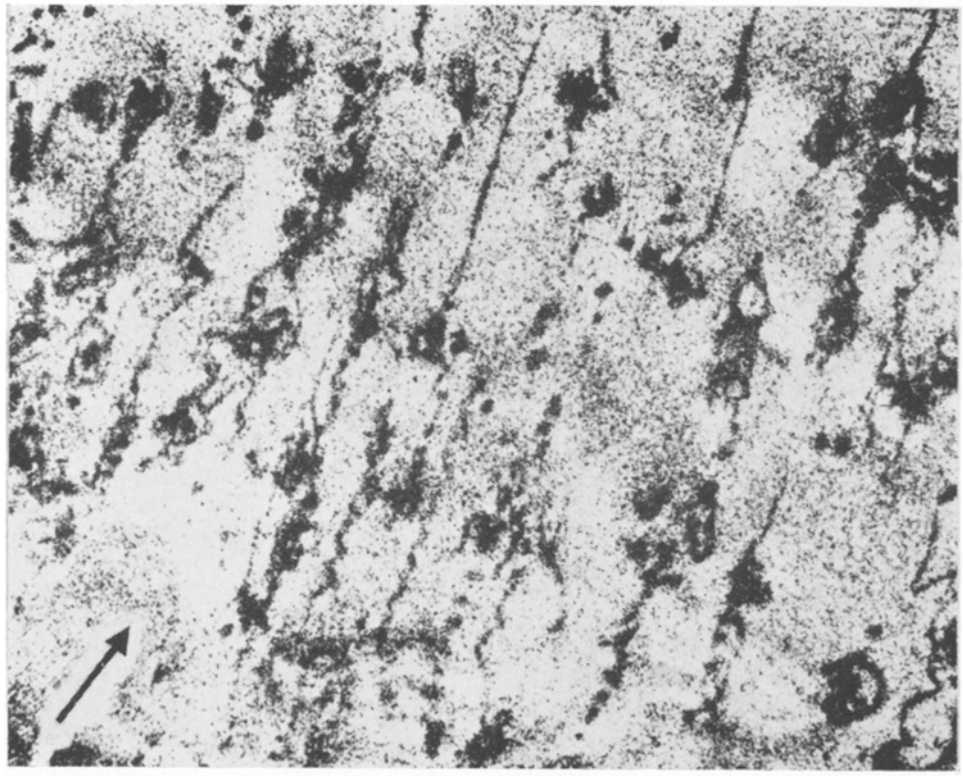

(b)

Figure 3 X-ray topographs of part of specimen A about 85 μm thick. AgKα radiation. Arrows, length 75 μm, indicate projection of **g**-vector on specimen surface: (a) 020 reflection (b) $\bar{1}01$ reflection. The features in fig. 3(a) indicated by letters on their left-hand sides are: A. an unresolved dislocation cluster, diameter 20 μm. B. a single dislocation loop, diameter in projection 15 μm. C. a dislocation cluster with loops resolved in its outer parts

uniform in thickness. The regions of darker background intensity seen on figs. 4a and b were about 65 to 75 μm thick.

The conspicuous features in fig. 3a are the discrete "clusters" of dislocations. The centres of the clusters are located with roughly equal density on both surfaces of the specimen: this is shown by stereo-pairs of topographs formed by hkl, $\overline{hkl}$ pairs of reflections [14]. There are about 75 clusters per mm^2 on each face, and the whole specimen area examined ($\sim \frac{1}{2}$ cm^2) was thus covered. The dislocations visible in fig. 3a have Burgers vectors in the $\langle 1\,1\,1 \rangle$ directions; in few clusters were not all four of these Burgers vectors represented, so it appeared from comparison of different reflections. In fig. 3a the average cluster diameter is about 30 μm. Individual dislocations resolved in the outer parts of clusters form irregular, non-planar loops. Many loops possess straight segments in the length range 10 to 15 μm. These resolved cluster dislocations exhibited some preference for lying in planes having orientations either near (0 1 0) or near that of the specimen surface.

A quite different dislocation pattern appears in fig. 3b. Now dislocations with [0 0 1] Burgers vector are visible. They are seen as rows of loops, and also as helices having a range of pitch angles and different degrees of regularity. The regular helices and the rows of small loops hold to the [0 0 1] direction closely as their axes; but helices of large and irregular pitch, and the occasional long straight segment, may deviate up to 30° from [0 0 1] orientation.

The relationship between the clusters (which are seen by themselves in the 0 2 0 reflection fig. 3a) and the dislocations with [0 0 1] Burgers vector, is again displayed in fig. 4a. In this $1\,\bar{2}\,\bar{1}$ reflection three out of four Burgers vectors of $\frac{1}{2}\langle 1\,1\,1 \rangle$ type are visible. One such, $\frac{1}{2}\langle 1\,\bar{1}\,\bar{1} \rangle$, gives $|\,\mathbf{g}\,.\,\mathbf{b}\,| = 2$ which condition produces a strong, thick image. This situation, coupled with the longer extinction distance of the $1\,\bar{2}\,\bar{1}$ reflection compared with those of the 0 2 0 and $\bar{1}\,0\,1$ reflections, accounts for the higher dislocation contrast but lower resolution in fig. 4a compared with the other figures. However, the pair formed by the $\bar{1}\,2\,1$ and $1\,\bar{2}\,\bar{1}$ topographs is particularly striking when viewed stereoscopically. It makes clearly evident the close parallelism with each other of all rows of coaxial loops, and it shows that many of these rows run from the centre of a cluster on one surface of the specimen right through to the other surface. The higher-resolution $\bar{1}\,0\,1$ reflection shows that loops with diameters of 5 μm and above take a variety of orientations when their separation substantially exceeds their diameter. The individual loops, the single turns of helices, and the individually resolved line segments within the clusters of $\frac{1}{2}\langle 1\,1\,1 \rangle$ Burgers-vector dislocations are of dimensions not much larger than the resolution limits of the topographs. Therefore close study of stereo-pairs by viewing the original L4 nuclear emulsion plates under twin microscopes was required to establish some of the details described above. Overlap between images of different dislocations belonging to the same cluster, and also with their attendant [0 0 1] Burgers vector loop and helix dislocations, prevented assignment of particular $\frac{1}{2}\langle 1\,1\,1 \rangle$-type Burgers vectors to individually resolved cluster dislocations in all but very few of the groups examined. An unambiguous Burgers vector identification was made on a comparatively large elliptical loop, 50 × 20 μm in size, lying approximately in (1 1 0) and situated about 200 μm outside the lower left edge of the field of fig. 4. This loop had a Burgers vector in the $[1\,\bar{1}\,1]$ direction, and since its long axis was perpendicular to this direction the loop was predominantly edge in character.

5. Edge Dislocation Arrays

Figs. 5a to d show the same region of specimen B at different times, and include different Bragg reflections. The field width and height are each about 1.75 mm. With the exception of parts near the top right and left corners of the field, the specimen thickness does not vary by more than about 25%, being in the range 105 to 135 μm. When interpretating the observed diffraction contrast features it is necessary to bear in mind the consequences of the relatively high X-ray absorption ($\mu t \sim 1.5$). Absorption, acting in conjunction with the image-diffusing effects of specimen thickness, causes a reduction of the contrast of dislocations which becomes more serious as their distance from the X-ray exit surface of the specimen increases. (Such changes in dislocation image quality in X-ray topographs of metal crystals have been previously described and illustrated [9, 12, 13].) Images of dislocations near the X-ray entrance surface are weak and diffuse compared with those near the exit surface. Hence it may be beneficial to rotate the specimen by 180° about the goniometer axis to interchange exit and entrance surfaces in order to improve the visibility and resolution of particular defects. As

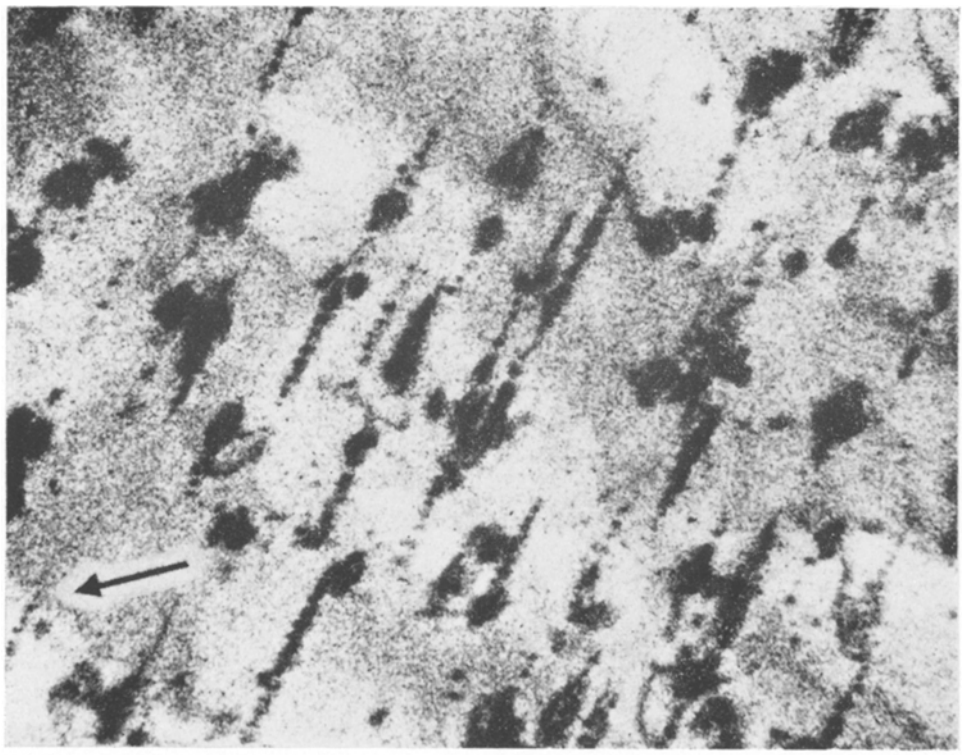

(a)

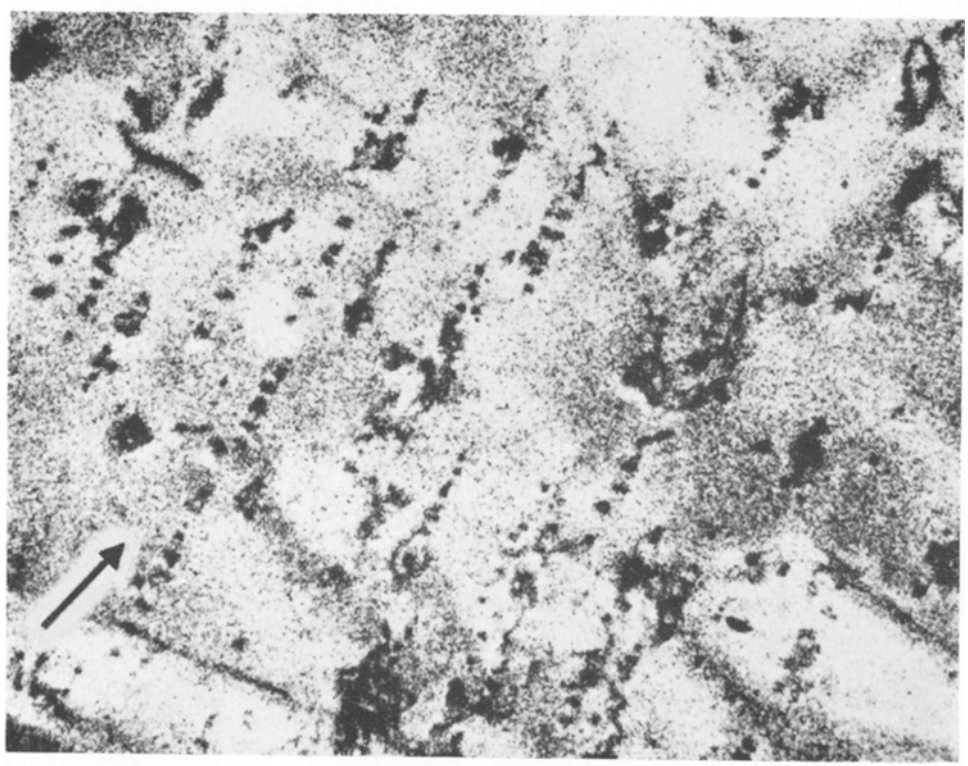

(b)

Figure 4 X-ray topographs of part of specimen A with thickness mainly between 65 and 75 μm. AgKα radiation. Arrows, length 75 μm, show projection of **g**-vector on specimen surface: (a) $1\bar{2}\bar{1}$ reflection. (b) $\bar{1}01$ reflection.

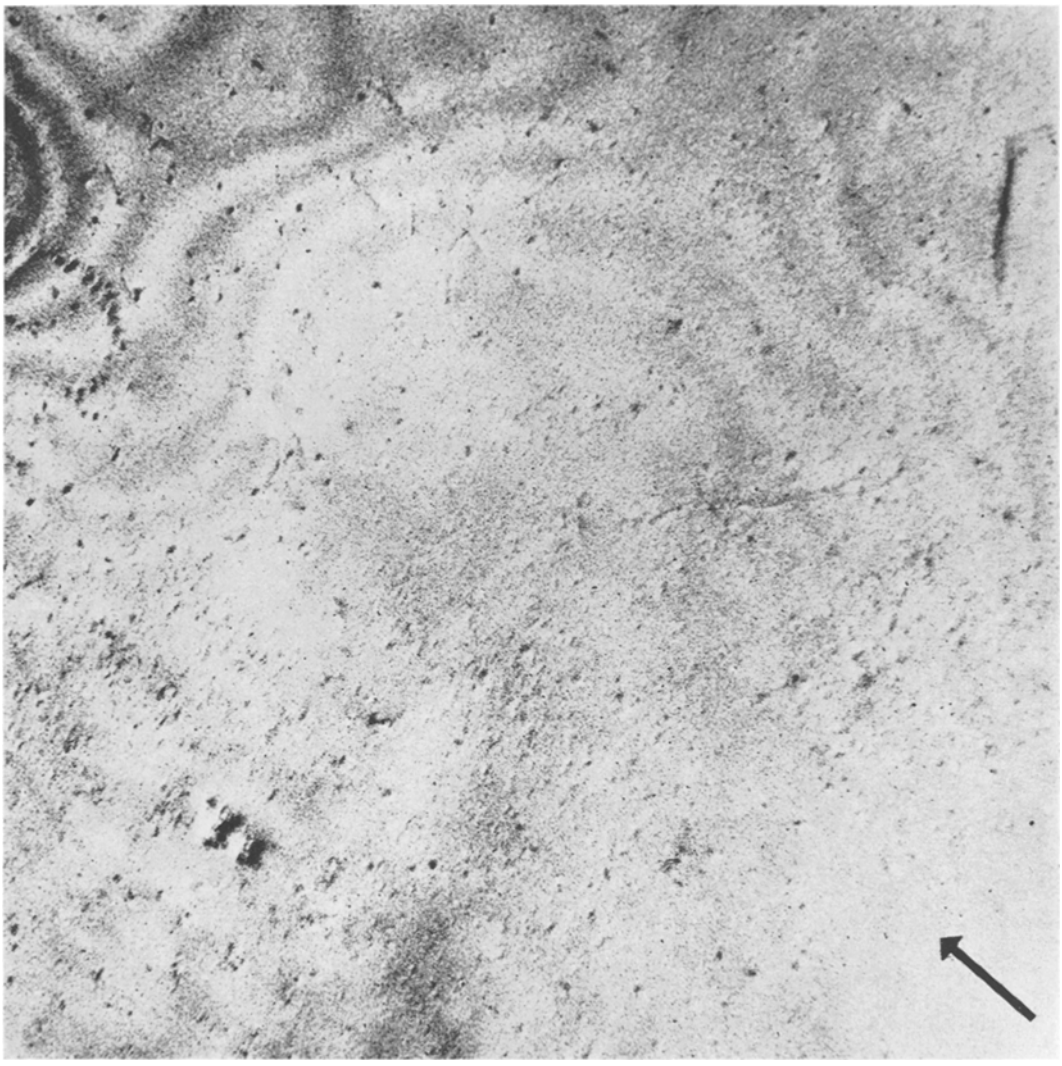

5(a)

Figure 5 Sequence of topographs of part of specimen B. AgKα radiation. Arrows indicate projection of **g**-vector on plane of specimen. Arrow length 200 μm: (a) 020 reflection. (b) repeat of (a) after interval of ten days. (c) $2\bar{2}0$ reflection, taken twenty days after (a) and with X-ray exit and entrance surfaces reversed relative to (a), (b) and (d). (d) $0\bar{1}1$ reflection.

an example, there are single dislocations whose images are weak and diffuse in fig. 5b which become strong and clear in fig. 5c. These dislocations lie close to the X-ray entrance surface when the specimen has its usual setting, as in fig. 5b. The topograph of fig. 5c was taken with exit and entrance surfaces interchanged, but in printing its photomicrograph left and right have been reversed so as to regain correspondence with figs. 5a, b and d. Noteworthy is the greater contrast and sharpness in fig. 5c of the dislocations with vertical and horizontal segments on the right of the centre. However, it should be added that their increased image strength arises in part because $\mathbf{g} \cdot \mathbf{b} = 2$ for these dislocations in the $2\bar{2}0$ reflection, as against $\mathbf{g} \cdot \mathbf{b} = 1$ in the 020 reflection.

Consider now the sequence figs. 5a to d. Fig. 5a was taken about one day after the specimen was prepared. The only recognisable dislocations are the pair of weak images running horizontally for about 0.4 mm from a point near the centre

Figure 5 continued 5(b)

out towards the right. The numerous specks arise mainly from defects at the specimen surfaces, although some small specks are produced by defects within the specimen, so the stereo-pairs show. On fig. 5a a vertical streak near the upper right margin was, in this field, the first to appear of a striking growth of dislocation arrays that developed spontaneously in the days that followed. After a lapse of ten days the growth rate of the arrays had become much slower: fig. 5b represents the condition then. The majority of the arrays, indeed all of those appearing in the field of fig. 5, lie parallel and close to the X-ray entrance surface of the specimen. Fig. 5c, taken with exit and entrance surfaces interchanged, shows the arrays more clearly and enables the individual dislocations in them to be resolved when their separation is 6 μm or more. The dislocations are extending downwards *en échelon*, the leader is on the right. In arrays on the other surface of the specimen, the pattern is related to that in figs. 5b and c by a rotation of 180°: the dislocations grow upwards *en échelon*, the leader on the left. Fig. 5c was taken ten days later than fig. 5b; the dislocation growth in this interval was noticeably less than in the interval between the topographs of figs. 5a and b. Indeed, in later topographs some of the single, vertical dislocation segments were seen to have started to shrink.

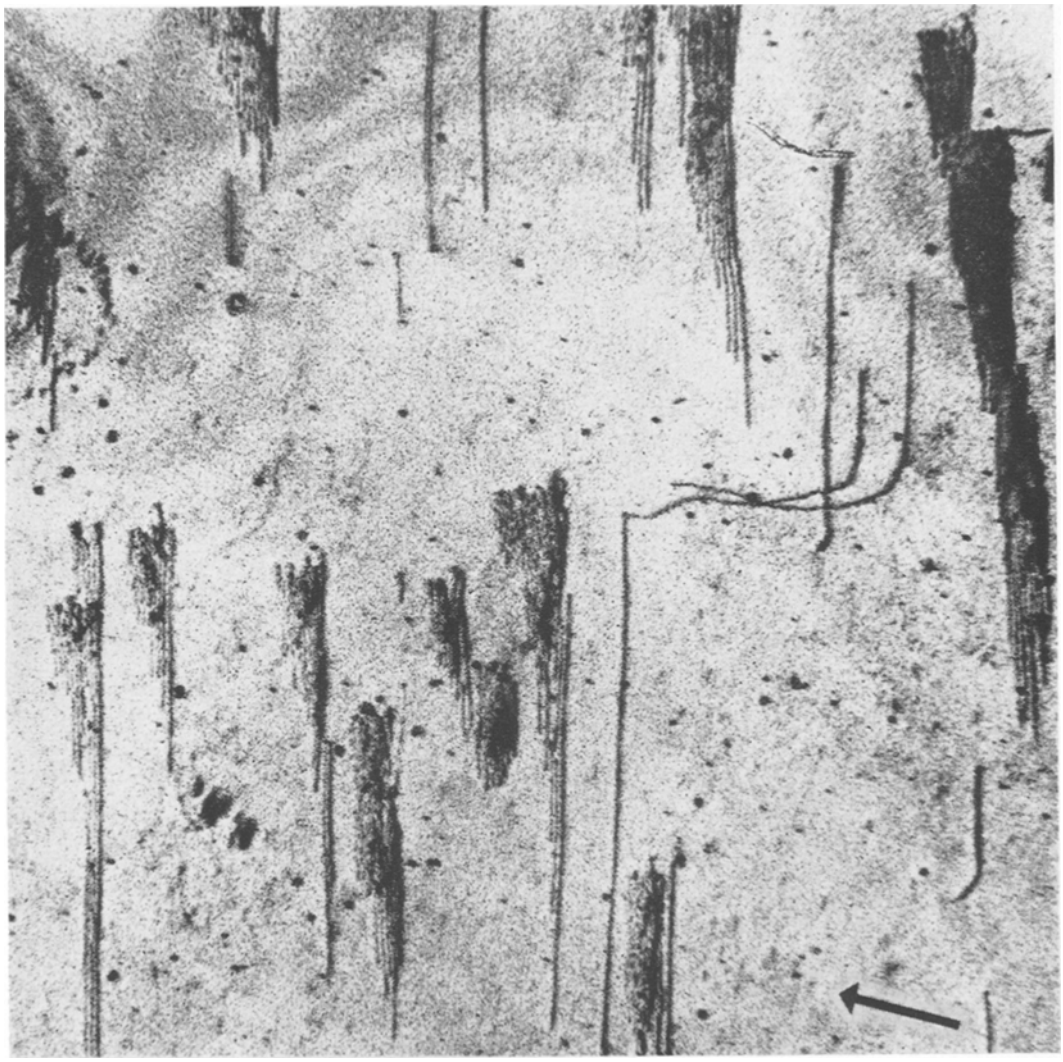

Figure 5 continued 5(c)

All the dislocations appearing in figs. 5b and c have Burgers vectors in the direction $[1\,\bar{1}\,\bar{1}]$. Their orientation in the plane of the specimen surface does not depart by more than about 3° from perpendicularity with $[1\,\bar{1}\,\bar{1}]$. They are thus of almost pure edge character. The Burgers vector identification was based on careful examination of dislocation image quality in the $\bar{1}01$ and $\bar{1}21$ reflections in addition to those here shown. Their very faint trace images in the $0\bar{1}1$ reflection, fig. 5d, is quite in accord with that expected from nearly pure edge dislocations with the stated Burgers vector and a 20° angle between the dislocation lines and the g-vector. The population of dislocations seen in fig. 5d as short lines trending from upper right to lower left all have [001] Burgers vector. Their mean direction lies in the plane containing [001] and the specimen surface normal, making about 45° with the latter.

The topographs cannot show with precision how far below the specimen surfaces lie the edge arrays, but they do allow bounds to be put on this distance. From the dislocation image contrast it is judged that the arrays lie at a depth probably between 2 and 4 μm below the surface.

The product μt in the field of fig. 5 is within the range favourable for the determination of the *sense* of the Burgers vectors of edge dislocations and of the stresses exerted on the substrate by

Figure 5 continued 5(d)

patches of imperfect crystal in the specimen surface [9, 12, 15]. (The determination takes advantage of the effects of lattice-plane curvature upon the X-ray energy-flow trajectories within the crystal [16].) An examination of all images produced by the arrays and single edge dislocations with $\frac{1}{2}[1\,\bar{1}\,\bar{1}]$ Burgers vector which formed the configurations under discussion, as they appeared in ten topographs taken under different conditions (such as hkl, $\bar{h}\bar{k}\bar{l}$ stereo-pairs of various reflections), demonstrated without exception that the sense of the Burgers vectors corresponded to the presence of a sheet of *vacancies* lying between the surface and the dislocation line.

6. Summary

The production of the loops and helices described in section 4 could possibly be due to punching by oxide particles attached to the specimen surfaces. It is to be noted that only the [001] Burgers-vector dislocations are involved in coaxial loop and helix formation. However, with no knowledge of the microscopic stress field responsible, in particular of what anisotropy it might possess, it would be unwise to regard this uniqueness as more than strongly suggestive of different nucleation and glide characteristics of dislocations with [001] Burgers vector compared with those of $\frac{1}{2}\langle 1\,1\,1\rangle$ Burgers vector type.

The growth of edge dislocations parallel to the

specimen surface, as discussed in section 6, was strongly manifested in one specimen (B), moderately in another,* and was absent in a third; yet all three specimens had received similar treatments. The nature of the surface conditions that favour these dislocation structures is at present unknown. That only one of the four $\frac{1}{2}\langle 111\rangle$-type Burgers vectors is involved must arise from the small angle, 5°, that the $[1\bar{1}\bar{1}]$ direction makes with the specimen surface. (The mean surface orientation lies between (211) and (311).) None of the other possible Burgers vectors make angles with the surface smaller than 32°. The size to which the edge arrays grew, each dislocation extending at an average rate of about 1 μm per hour over a period of weeks, is remarkable. The only comparable observations known to the authors are those of Michell and Ogilvie who studied by X-ray topography the growth of large dislocation networks and loops lying in (0001) planes of zinc and cadmium crystals of (0001) plate habit after exposure to air [17].

Acknowledgement

The authors express their thanks to Mr J. H. Burrow for constructing the melt filtration apparatus and the furnace vacuum vessel, and to the Royal Society for the financial support that enabled one author (RF) to work in Bristol.

References

1. H. TAKAKI, M. KOYAMA, Y. TSUJII, and S. MAEDA, *Trans. Japan Inst. Metals* **8** (1967) 195.
2. E. TEGHTSOONIAN and B. CHALMERS, *Can. J. Phys.* **29** (1951) 370.
3. T. S. NOGGLE, *Rev. Sci. Instrum.* **24** (1953) 184.
4. D. JAFFREY and D. A. CHADWICK, *Phil. Mag.* **18** (1968) 573.
5. L. G. SCHULZ, *Trans. AIME* **200** (1954) 1082.
6. O. BRÜMMER and V. ALEX, *Phys. stat. sol.* (a) **3** (1970) 193.
7. A. R. LANG, *Acta Cryst.* **12** (1959) 249.
8. W. B. PEARSON, "Handbook of Lattice Spacings and Structures of Metals", Vol. II (Pergamon Press, Oxford, 1967) p. 89.
9. A. R. LANG and M. POLCAROVÁ, *Proc. Roy. Soc.* **A 285** (1965) 297.
10. S. A. BRADFORD and R. W. VIETH, *Trans. Met. Soc. AIME* **236** (1966) 232.
11. L. R. WOODYATT and S. A. BRADFORD, "Revised Angular Tables for Beta Tin" (File ref. 1828, Homer Research Laboratories, Bethlehem Steel Corpn., Bethlehem, Pa., 1966).
12. A. R. LANG, in "Modern Diffraction and Imaging Techniques in Material Science", edited by S. Amelinckx, R. Gevers, G. Remaut, and J. Van Landuyt (North-Holland Publishing Co., Amsterdam-London, 1970) 407.
13. M. POLCAROVÁ and A. R. LANG, *Phys. stat. sol.* (a) **4** (1971) 491.
14. A. R. LANG, *J. Appl. Phys.* **30** (1959) 1748.
15. F. C. FRANK, B. R. LAWN, A. R. LANG, and E. M. WILKS, *Proc. Roy. Soc.* **A301** (1967) 239.
16. P. PENNING and D. POLDER, *Philips Res. Reports* **16** (1961) 419.
17. D. MICHELL and G. J. OGILVIE, *Phys. stat. sol.* **15** (1966) 83.

Received 7 October and accepted 26 October 1971.

*No arrays like those in fig. 5 appeared in this specimen. Its dislocation density was higher. Outcropping dislocations with $[1\bar{1}\bar{1}]$ Burgers vector direction tended to extend in pure edge orientation parallel to and just below the surfaces.